

Zircon ages from suspended load as tracers for the inversion of subglacial erosion rates.

Bruno Belotti

Under the direction of Prof. Frédéric Herman



Photo: Bruno Belotti





UNIL | Université de Lausanne

Ce travail n'a pas été rédigé en vue d'une publication, d'une édition ou diffusion. Son format et tout ou partie de son contenu répondent donc à cet état de fait. Les contenus n'engagent pas l'Université de Lausanne. Ce travail n'en est pas moins soumis aux règles sur le droit d'auteur. À ce titre, les citations tirées du présent mémoire ne sont autorisées que dans la mesure où la source et le nom de l'auteur·e sont clairement cités. La loi fédérale sur le droit d'auteur est en outre applicable.



Zircon ages from suspended load as tracers for the inversion of subglacial erosion rates.

Bruno Belotti

Faculty of Geosciences and Environment - University of Lausanne, Switzerland

Under the supervision of Prof. Frédéric Herman

Abstract

By means of subglacial processes such as abrasion and quarrying, Alpine glaciers actively erode the underlying bedrock and mobilize large amounts of sediments. Glacial erosion rates are commonly linked to basal sliding and rock erodibility, but precise controls on its spatial variability and short-term dynamics within a glacier are yet to be robustly constrained. Here we determine the provenance of zircon grains found suspended in the proglacial stream using an inversion approach to establish spatial patterns of erosion below a glacier and their evolution in time via repeated sampling throughout the early melting season. We focus on the Gornergletscher glacial system (Swiss Alps), which is one of the fastest fast-flowing glaciers in the Alps. It is also rapidly retreating in response to global warming. Thereby, we generate time-series of erosion maps, which are presented here in hourly resolution for two days during summer 2019. The inferred erosion maps show that sediment delivery during the early melting season is strongly influenced by the sudden activation of sediment supply zones, and that erosion rates evolve throughout the day along with discharge. Areas that were recently exposed by the glacier's retreat appear to be major erosion sources, and their signal is clearly dominant over that of glacial erosion for the concerned spatial units.

Contents	References	13
1 Introduction	1	
2 Geological setting and sampling	3	
3 Methods	3	
3.1 Determination of zircon ages	3	
3.1.1 Grain selection and preparation	3	
3.1.2 SEM-CL	3	
3.1.3 LA-ICPMS	3	
3.2 Inversion of zircon ages	4	
4 Limitations	6	
5 Results and discussion	6	
5.1 LA-ICPMS zircon age signatures	6	
5.2 Erosion rates	7	
5.2.1 Deposited detrital samples	9	
5.2.2 Suspended detrital samples	10	
5.2.3 Ice velocities and slope contribution	10	
6 Conclusions	12	
7 Data availability	13	
8 Acknowledgements	13	

1 Introduction

By means of subglacial processes, such as abrasion and quarrying, Alpine glaciers actively erode the underlying bedrock and mobilize large amounts of sediments. Glacial erosion rates can be linked to basal sliding velocities and rock erodibility by means of the following heuristic rule (Hallet, 1979; Herman et al., 2015; Koppes et al., 2015; Herman et al., 2018):

$$\dot{e} = K_g |u_s|^l \quad [1]$$

where \dot{e} is the erosion rate, K_g is a proportionality constant, u_s is the basal sliding velocity, and l is an exponent, but precise controls on glacial erosion and its spatio-temporal variability are yet to be consistently constrained. A better understanding of such processes and their reaction to current climate change is important for forecasting future sediment yield in Alpine regions, where glacial meltwater is largely employed for hydropower production, and sediments make the object of extensive management (Schaefer et al., 2007). Glacial erosion has previously been studied by means of catchment integrated mean erosion rates from sed-

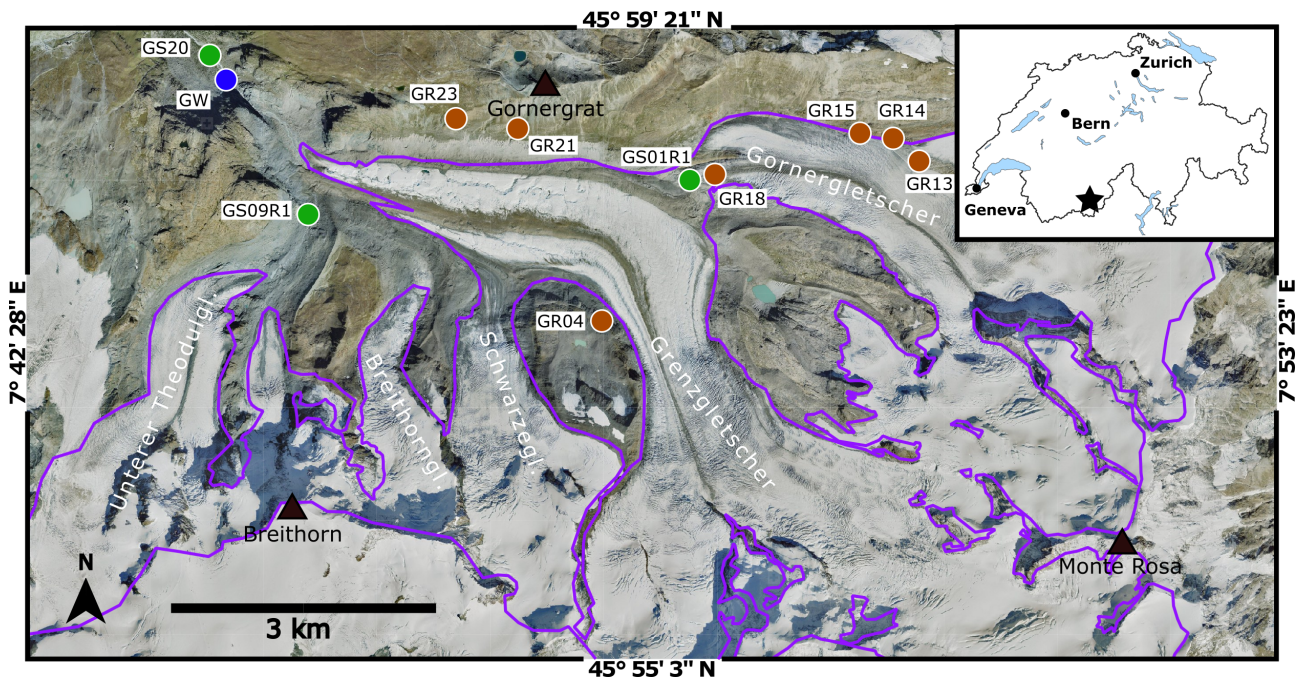


Figure 1: Gorner glacial system (Swisstopo, 2021). Purple contours represent glacial extent of 2018. Brown and green circles represent bedrock and detrital sediments sampling locations respectively. The blue circle represents the approximate position of the water (suspended load) sampling location.

iment loads (e.g., Collins, 1990; Hallet et al., 2013; Delaney et al., 2018) or modelling studies (e.g. Hallet, 1996; MacGregor et al., 2009; Ugelvig et al., 2016). Although these studies provided key insights, they did not offer intra-catchment information about the controls on spatial (and short-time temporal) variability of erosion rates, and the latter lack observations to back up the theory. The distinction of different erosion processes within a glacierized catchment has already been investigated through *in situ* experiments (e.g. Guillon et al., 2015), coupled with sediment fingerprinting for the location of different source areas and their main erosion-driving processes (e.g. Tsyplenkov et al., 2021). However, studies distinguishing different subglacial source areas and their contribution on sub-daily to seasonal timescales are missing.

Here, subglacial erosion is investigated at the glacier scale by means of sediment fingerprinting (Koiter et al., 2013) using zircon age signatures from both suspended and deposited grains in the proglacial stream, and an inversion approach (based on De Doncker et al., 2020) is used to unmix the amalgamation of tracers in the resulting sediment record. In addition to the reconstruction of spatially varying subglacial processes, the unprecedented use of fingerprints from suspended load in the proglacial stream allows for the interpretation of temporal variations in erosion rates (and sediment mobilization).

Detrital zircons are often used as fingerprints for provenance analysis (Gehrels, 2011) because of their omnipresence in the Earth's crust (common trace elements

in magmatic rocks), versatility and low alteration and disturbance over time. Single grain U/Pb geochronology became increasingly used after the advent of Laser-Ablation Inductively Coupled Plasma Mass Spectrometry (LA-ICPMS), which is methodically similar to Secondary Ion Mass Spectrometry (SIMS), but allows for faster analysis times (Gehrels, 2011). Common problems for the assessment of absolute ages such as re-crystallisation and Pb loss/inheritance do not negatively influence this study's results as long as these are internally homogeneous for each source area. The fingerprinting method relies on the fact that different geological units have their own tectono-sedimentary histories and therefore feature unique U/Pb age signatures, which strengthens the choice of zircon ages as fingerprints. This study assesses the suitability of zircon age signatures as tracers for sediment fingerprinting by means of an inverse erosion model, and evaluates this method's effectiveness for detecting spatial variability in sediment delivery at a single glacier complex scale. The Gornergletscher (Fig. 1), canton of Valais, Switzerland, was chosen as study site because of its convenient geological substrate (composed of a known distribution of heterogeneous lithologies), its accessibility and its long-standing scientific record.

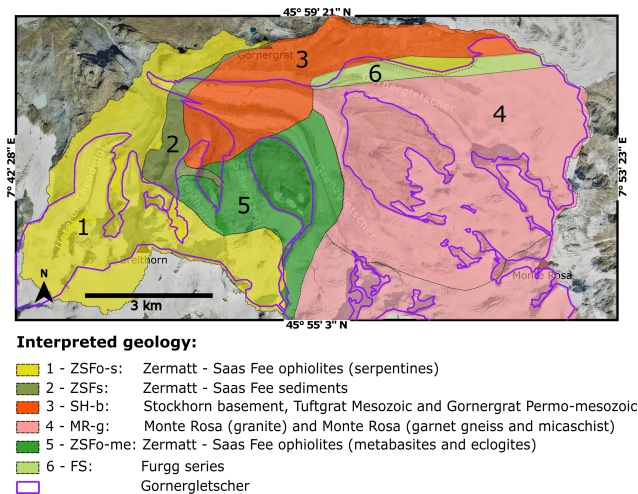


Figure 2: Subglacial geology according to the interpretation proposed by De Doncker (2019) with the assistance of Lukas Baumgartner (UNIL, ISTE) (modified from Steck et al., 2015; De Doncker et al., 2020).

2 Geological setting and sampling

The Gorner glacier is part of a glacial system comprising five tributaries lying between 2200 m and 4600 m above sea level and covering an area of approximately 50 km² (Fig. 1). The glacial system features a known heterogeneous subglacial bedrock, making it suitable for the fingerprinting approach. Fig. 2 shows the area's geological units and the projected interpretation of their subglacial distribution (De Doncker, 2019). Bedrock samples were gathered from outcrops on each geological unit (Fig. 1) except for the Monte-Rosa garnet gneiss and micaschist unit, that is assumed to be equal to the rest of the Monte Rosa unit regarding its zircon signature. This study assumes internally homogeneous geological units in terms of zircon fertility, although it is known that parent rock zircon fertility can internally change by several orders of magnitude, making it a major source of bias in detrital geochronology (Malusà et al., 2016).

Deposited sediments were gathered on sandy banks along the proglacial stream (Fig. 1). Suspended sediments were extracted from water samples collected by means of a normed manual inlet (integrating suspended-load bottle sampler) in the Gornera stream at approximately 1.5 km down-valley from the 2019 glacier terminus. Suspended sediments were sampled on June 05, 2019 and June 28, 2019. Simultaneous turbidity and discharge measurements are available for both days, and Fig. 3 shows temperature, precipitation and discharge situations throughout the sampling period. Both sampling dates (red dots in Fig. 3) were preceded by many days of regular temperatures and discharge with no precipitation, although a heavy rain-

fall event took place between them on June 10 - June 12, which nearly doubled the river's peak discharge. An important temperature raise from June 23 resulted in average discharges that are twice as high on the second sampling day (June 28) compared to the first (June 5).

3 Methods

Analyses and processing were performed in two distinct phases: 1) sample preparation and laboratory analyses for the measurement of zircon ages; 2) Post-processing and modelling on "MATLAB" (2018).

3.1 Determination of zircon ages

3.1.1 Grain selection and preparation

Sample preparation and analysis was carried out following Aoki et al. (2019) and (when suitable) Andersen (2005): Zircon grains were extracted from bedrock and detrital samples by means of traditional heavy liquid mineral separation after crushing (or filtering, for suspended sediment samples). Single grains of similar size were then manually selected from each sample under an optical microscope and prepared into polished epoxy mounts for *in situ* LA-ICPMS at UNIL's laboratories. Although, because of time constraints, a comprehensive analysis of grain sizes (and the subsequent selection of representative populations as recommended by Andersen, 2005) was not possible, up to three separate grain sizes were mounted for samples where zircons were scarcest and/or where bi/multi-modal size distributions were clearly present.

3.1.2 SEM-CL

Cathodoluminescence (CL) images were obtained with a CamScan MV2300 Scanning Electron Microscope (SEM) and used for the interpretation of each crystals' internal structure and to avoid inclusions, metamictic areas and mixed age domains during the placement of ablation spots (Fig. 4) (Schoene, 2014; Gehrels, 2011). This step revealed generalized metamictisation in bedrock sample GR23.

Laser spot diameters varied between 20 - 30 μm depending on grain size.

3.1.3 LA-ICPMS

LA-ICPMS was carried out by means of a sector-field Element XR spectrometer and an ArF RESOLUTION 193 excimer LA system. Primary and secondary reference zircons were (respectively) GEMOC GJ-1 (CA-ID-TIMS ²⁰⁶Pb/²³⁸U age of 600.5 ± 0.4 Ma, Horstwood et al., 2016) and Plešovice (337.207 ± 0.029 Ma, Widmann et al., 2019). Data was reduced using LAMTRACE (Jackson, 2008). Table 1 resumes the details for each sample. Approximately 750 zircon crystals were processed this way in total. Since the goal

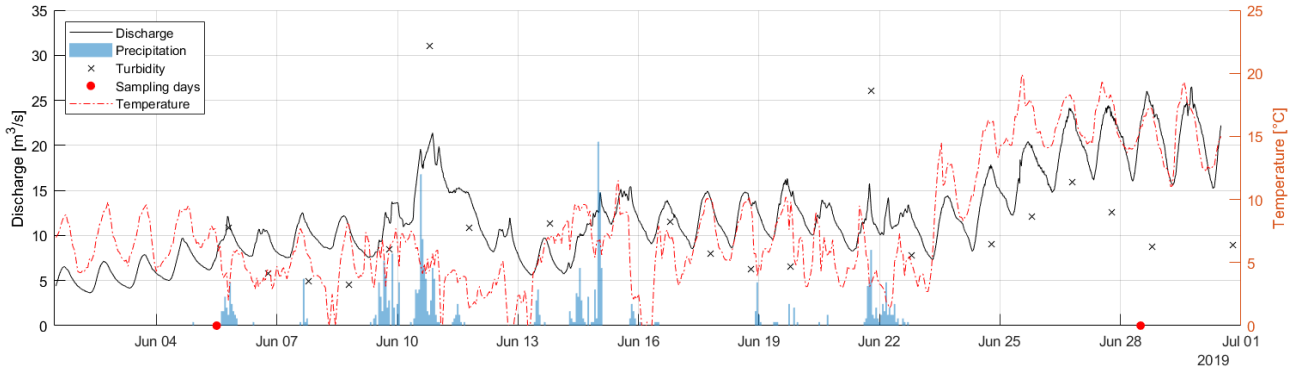


Figure 3: Air temperature, precipitation at Gornergletscher; discharge and turbidity as measured in the Gornera river. June 2019 (FOEN, n.d.; Prasicek et al., 2020)

Sample type	Source (bedrock)/ date (detrital)	Sample ID	Sample weight [g]	Zircon fertility [ppm]*	Total zircons [#]	Selected zircons [#]	Average grain size [μm]
Bedrock	1 - ZSFo-s	GR15	855	0.021	40	10 - 1 (11)	45 - 55
	2 - ZSFs	GR23	850	0.149	1000	60	30
	3 - SH-b	GR21	1070	9.346	6200*	99	70
	4 - MR-g	GR13	480	10.417	4900*	106	60
	5 - ZSFo-me	GR04	115	0	0	0	-
	6 - FS	GR14	310	3.790	2000	100	50
Sand	Summer 2018	GS01R1	31	1.8	100	35 - 9 (44)	55 - 50
	Summer 2018	GS09R1	25	35.9	2000	100	50
	Summer 2019	GS20	1310	7.6	10 mg	100	60
Water	05.06.19 - 13:30	GW27	0.16	77.0	80	8	35
	05.06.19 - 15:00	GW29	0.12	95.7	50	8	40
	28.06.19 - 10:30	GW22	0.24	41.7	65	19	35
	28.06.19 - 12:30	GW21	0.32	45.3	100	21 - 1 (22)	35 - 20
	28.06.19 - 13:30	GW23	0.41	34.8	60	14 - 8 (22)	35 - 50
	28.06.19 - 14:30	GW25	0.40	63.3	175	20 - 15 - 1 (36)	30 - 40 - 55

Table 1: Detailed sample information. Multiple values in the “selected zircons” column indicate that more than one grain size was analysed; grain sizes are specified in the following column. Note that weights of water samples correspond to the filtered and dried sediments. See Fig. 2 for the full names of geological units (*calculated values).

of this method is to get a unique tectonic fingerprint for each unit, discordant results were not excluded from the dataset as long as no evident common lead contamination, mixed age domains or intrusions were detected during reduction (except in extreme cases).

3.2 Inversion of zircon ages

Supposing that each source area (lithological unit) has its unique fingerprint which is not altered during erosion and transport, the contribution of each source to the resulting detrital data can be estimated. Here we first acquire information on the zircon age-distribution and zircon concentration of each unit, i.e. source, and then collect sediments in the main stream. Erosion rates can then be inferred using a Bayesian approach, which includes a prior estimation of erosion, and a forward model that enables to map the bedrock erosion into a probability distribution of zircon ages. We follow the approach introduced by De Doncker et al. (2020), which has already been used on synthetic and natural data. The forward model can be expressed

as follows:

$$\begin{bmatrix} d_1 \\ d_2 \\ \vdots \\ d_n \end{bmatrix} + \epsilon = \begin{bmatrix} g_{1,1} & g_{1,2} & \cdots & g_{1,m} \\ g_{2,1} & \ddots & & \vdots \\ \vdots & & \ddots & \vdots \\ g_{n,1} & \cdots & \cdots & g_{n,m} \end{bmatrix} \cdot \begin{bmatrix} \dot{e}_1 \\ \dot{e}_2 \\ \vdots \\ \dot{e}_m \end{bmatrix} \quad [2]$$

where d is the resulting data (tracer concentrations), ϵ is the error, G is a matrix containing tracer concentrations for every discrete surface unit, \dot{e} is the erosion rate, n is the number of tracers (zircon age bins), and m is the number of cells in the erosion rate map.

Note that the inversion scheme corresponds to the least-squares method (as described by Tarantola & Valette, 1982) and uses prior erosion estimates (e.g. average catchment erosion) to infer the model parameters via Bayesian probability.

In turn, we solve the following equation:

$$\dot{e}_{post} = \dot{e}_{pr} + C_m G^T (G C_m G^T + C_d)^{-1} (d - G \dot{e}_{pr}) \quad [3]$$



Figure 4: Examples of cathodoluminescence results and ablation spots selection for bedrock (GR), deposited (GS) and suspended (GW) zircons. Spot sizes are 30 μm for GR13 and GS09R1, and 20 μm for GW23. All ages are calculated from $^{206}\text{Pb}/^{238}\text{U}$ ratios.

where \hat{e}_{post} is the posterior erosion rate, \hat{e}_{pr} is a prior erosion rate, C_m is the model covariance and C_d is the data covariance. The prior erosion rate is set equal to the mean erosion rate of the catchment, computed as the volume of sediments exported in the meltwater river during one year - derived from calibrated turbidity measurements (Prasicek et al., 2020) - divided by the total area of the catchment.

The model covariance in [3] is calculated as:

$$C_{m(i,j)} = \sigma_m^2 \exp\left(-\frac{d_{(i,j)}^2}{\lambda^2}\right) \quad [4]$$

where σ_m is the standard deviation of the prior erosion rate, $d_{(i,j)}$ is the euclidean distance between pixels and λ is the smoothing distance.

This parameter accounts for the spatial relations between sediment sources, and allows for a modifiable smoothing distance. The data covariance in [3] is calculated as:

$$C_d = \sigma_d^2 I \quad [5]$$

where σ_d^2 is the data variance and I is an identity matrix. To impose a positivity constraint, the model is non-linearized by taking the logarithm of the forward statement. The inverse problem is then solved using the steepest descent method following Tarantola (2005).

It is worth stressing that fingerprints are the zircon-age distributions (scaled by the zircon concentrations) of each lithological unit. Since every source area has its unique fingerprint, through differential glacial erosion (and transport), suspended load data is expected to contain zircons of different ages in different concentrations, reflecting the differential erosion of the source areas. This means that the elements of the forward model in [2] are no longer predetermined in the inverse problem: G (the spatial distribution of fingerprints) is known, and d (the resulting detrital data) is measured, but \hat{e} (the erosion rates for each cell in the model) is unknown. More specifically, the zircon-age spectra of each geological unit (or source area) are divided into age bins. As such, every geological unit contains tracers - zircons of a certain age bin - in a certain concentration. These tracers are passively transported downstream suspended in water, and G can be seen as a stack of tracer concentration maps. Importantly, the internal variability of zircon fertilities within each geological unit - source area - is assumed to be zero.

While G and \hat{e} in both [2] and [3] can be intuitively pictured as maps (respectively, one concentration [ppm] and one erosion [$\frac{\text{mm}}{\text{yr}}$] value for each discrete spatial cell of the model), the elements of vector d (that displays the measured "tracer concentrations" of the detrital samples, which are also the main input of the inverse model) are composite values.

Here, these tracers correspond to $n = 13$ “age bins” (in Myr: 40-140; 140-200; 200-210; 210-250; 250-263; 263-270; 270-340; 340-430; 430-475; 475-555; 555-585; 585-750; 750-800), which are specific age intervals chosen by manually clustering the spectrum of resulting ages (Fig. 5) from all samples into distinct age-bins. Therefore, each element in d is the percentage of zircons in one specific sample whose measured ages fall within the interval of each age bin. These percentages are then weighted by multiplying them times their zircon concentration (fertility) [ppm] in the total sampled material (calculated from estimates of the total mass of zircon in each bedrock/sediment sample). This returns quantities that are directly comparable with the source tracer concentrations in G , hence allowing for the computation of \dot{e} . The zircon age distributions are scaled with parent rock zircon fertilities in order to correct for zircon concentration effects. Information on parent rock zircon fertilities can be obtained by means of chemical analyses on bedrock samples, but this method returned fertilities that differ strongly from the zircon concentration in the bedrock samples as calculated from the size and total number of extracted zircon grains. Such contradictory concentrations might be explained by internally heterogeneous zircon fertilities (Malusà et al., 2016), and biases during zircon separation and grain selection. Parent rock zircon fertilities as measured from chemical analyses were hence considered not representative of the sampled material from which zircons were extracted for geochronology, therefore fertilities calculated from extracted zircon quantities were used instead.

4 Limitations

Given the nature of this study’s fingerprints, and because of the limited understanding of basal sediment storage (and its evolution), and mobilization at the glacier scale, the results discussed below should be interpreted with caution: although it is true that the presence of suspended tracers in the proglacial stream could arguably be attributed to direct glacial erosion, the same controlling factors on erosion investigated here - i.e. temperature and discharge variations, as well as catchment slope and (indirectly) ice surface velocities - are known to affect subglacial sediment dynamics such as storage, (re)mobilization and transport (Gurnell et al., 1996; Swift et al., 2005; Haritashya et al., 2010). Therefore, interpretation of the resulting erosion rate maps needs to be done with care, as the model shows sediment delivery rates that can include both the reworking of previously deposited sediments as well as direct delivery of sediments sourced by bedrock erosion or hillslope erosion. Furthermore, the only prior information input in the model is the mean erosion rate. No prior information on sediment storage or glacier geometry is given; the model returns erosion rates to match detrital data with fingerprint concen-

tration maps. As discussed in section 5.2, smoothing is needed because the problem is under-determined, meaning that the resulting patterns of erosion rates at the individual gridcell-scale correspond to a spatial averaging of the solution. The smoothing constraint should be kept in mind when investigating the spatial relationship between erosion rates and other spatially varying processes such as ice sliding velocities, slope and elevation. The Gorner glacier is also known for other paraglacial processes such as the periodical formation and drainage of the glacier-dammed lake *Gornersee* (Sugiyama et al., 2008), which adds further complexity to the system by the sudden flushing out of stored sediments and the reorganisation of the subglacial drainage network.

Thus, results are most likely a combination (to an unknown ratio) of 1) simultaneous glacial erosion, and 2) remobilization of formerly eroded and stored sediments. Furthermore, subglacial transit times for sediments from different parts of the system are unknown for the investigated period, but might differ significantly (Werder et al., 2010, show that in July 2006 and in normal weather conditions a water parcel entering the glacier at the Gorner-Grenz intersection might have had to transit for over 150 minutes before leaving the subglacial channel system). It is thus likely that sediments eroded or mobilized at different times might coexist in the suspended load samples, and a general delay between erosion and its detection in the proglacial stream is expected.

5 Results and discussion

5.1 LA-ICPMS zircon age signatures

Results of geochronology on zircon crystals are presented in Fig. 5. Availability of geochronology data such as complete LA-ICPMS results and concordia diagrams for each bedrock sample are presented in section 7.

Age distributions of bedrock samples show distinct groups for almost all units except unit 1 (Zermatt - Saas Fee ophiolites: serpentines), which only yielded few zircons and with inconsistent ages, and unit 5 (Zermatt - Saas Fee ophiolites: metabasites and eclogites) for which no zircons were found. The resulting age signals are easily distinguishable and no spike overlaps are observed: this is an optimal outcome for the generation of unique fingerprints, which led to a straightforward separation into age bins (for which the statistical difference was confirmed at 1% significance level by a Kruskal-Wallis test). Detrital zircons from both suspended and deposited sediments reflect the abundance of grains from the Monte Rosa unit, while the remaining ages seem under-represented. After weighting each sample with its specific zircon fertility and after separating the distributions into age bins, these detrital age signatures did yield erosion rates time-series that

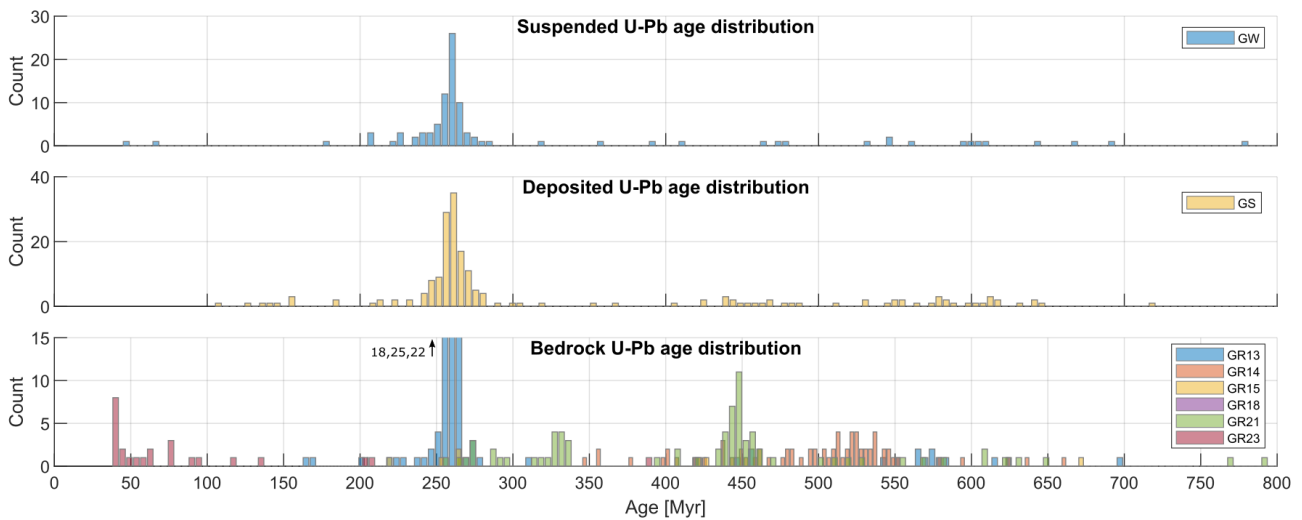


Figure 5: LA-ICPMS measured age signatures at 5 Myr resolution. GR04 was omitted as it contained no zircon grains. Suspended and deposited detrital ages are shown without distinction between samples. Note that data is not yet weighted for source fertility.

are remarkably consistent in space and time.

5.2 Erosion rates

The spatio-temporal variations of erosion rates were reconstructed via this unprecedented method over monthly (June 5 to June 28, 2019) and hourly (several states within each day of sampling) intervals, yielding promising results (Fig. 6). The model's results are one erosion map per detrital sample (Fig. 6) where colors indicate spatially varying erosion rates [$\frac{mm}{yr}$]. Fig. 8 shows the same results, but with normalized average values for each unit, to be read as the relative contribution of each unit to total erosion through time. Inversion is done without information on glacier boundaries, meaning that the presence and geometry of ice, unlike that of the geological units, does not impact the geometry of the resulting erosion rates. Rather, the resulting erosion rate maps stem from each unit's individual result and their vicinity to other units to a degree controlled by the model's covariance C_m in [5] (namely, by the euclidean distance between the model's cells, and the selected smoothing distance λ , that is 1200 m as recommended by De Doncker et al., 2020). This explains why the shapes of the original geological units (also displayed on Fig. 6) are easily recognizable in the inversion results.

As mentioned in section 4, even though the resulting values are expressed as erosion rates, one should interpret these as sediment delivery patterns. The three main sources that can deliver sediments are 1) glacial bedrock erosion with direct transport of the generated sediments, 2) flushing out of subglacially deposited sediments, 3) erosional processes in the paraglacial domain (by mass wasting or river incision). The contribution of these three sources depends on the sediment availability and the transport capacity in each of these do-

mains. Importantly, given the strong rainfall events, such as on June 9-10 2019, and the subsequent sharp increase in discharge (Fig. 3), coupled with the inefficient subglacial drainage system typical of the early melting season (Swift et al., 2005), it is possible that on June 28 the subglacial sediment stocks were exhausted and too little precipitation was available for hillslope erosion in the paraglacial domain. The erosion rate maps for June 28 could therefore correspond to direct transport of eroded glacial sediments, combined with reworking of sediments in the proglacial domain by the stream. The possible flushing out of a significant part of the sediments accumulated at the ice-bedrock interface during winter is suggested by the strong peak in turbidity measured during the same rainfall event by Prasicek et al. (2020), featuring the highest suspended sediment concentrations (SSCs) of the melting season (Fig. 3).

Interestingly, all resulting maps present the highest erosion rates on the western part of the catchment, more specifically on unit 1 (ZSFo-s), also visible in Fig. 8. Although it is not inconceivable that the two small, steep glaciers that flow on unit 1 (*Unterer Theodulgletscher* and *Triftjigletscher*) are responsible for the highest erosion rates in the glacial system, if it is assumed that glacial bedrock erosion were the dominant sediment source, such signals would rather be expected from areas featuring deeper ice such as the central/upper part of Gorner-Grenz tongue (flowing east to west, Eisen et al., 2009) or where the ice slides the fastest in the steep, narrowest part of Grenz glacier (Fig. 10). Such an unexpected result is presumably due to influences of sediment remobilization in the proglacial area: unit 1 is the closest to the sampling site (which was located directly downstream of it, Fig. 1), and is characterized by a large availability of materials from *in situ* erosion because of the glacier's

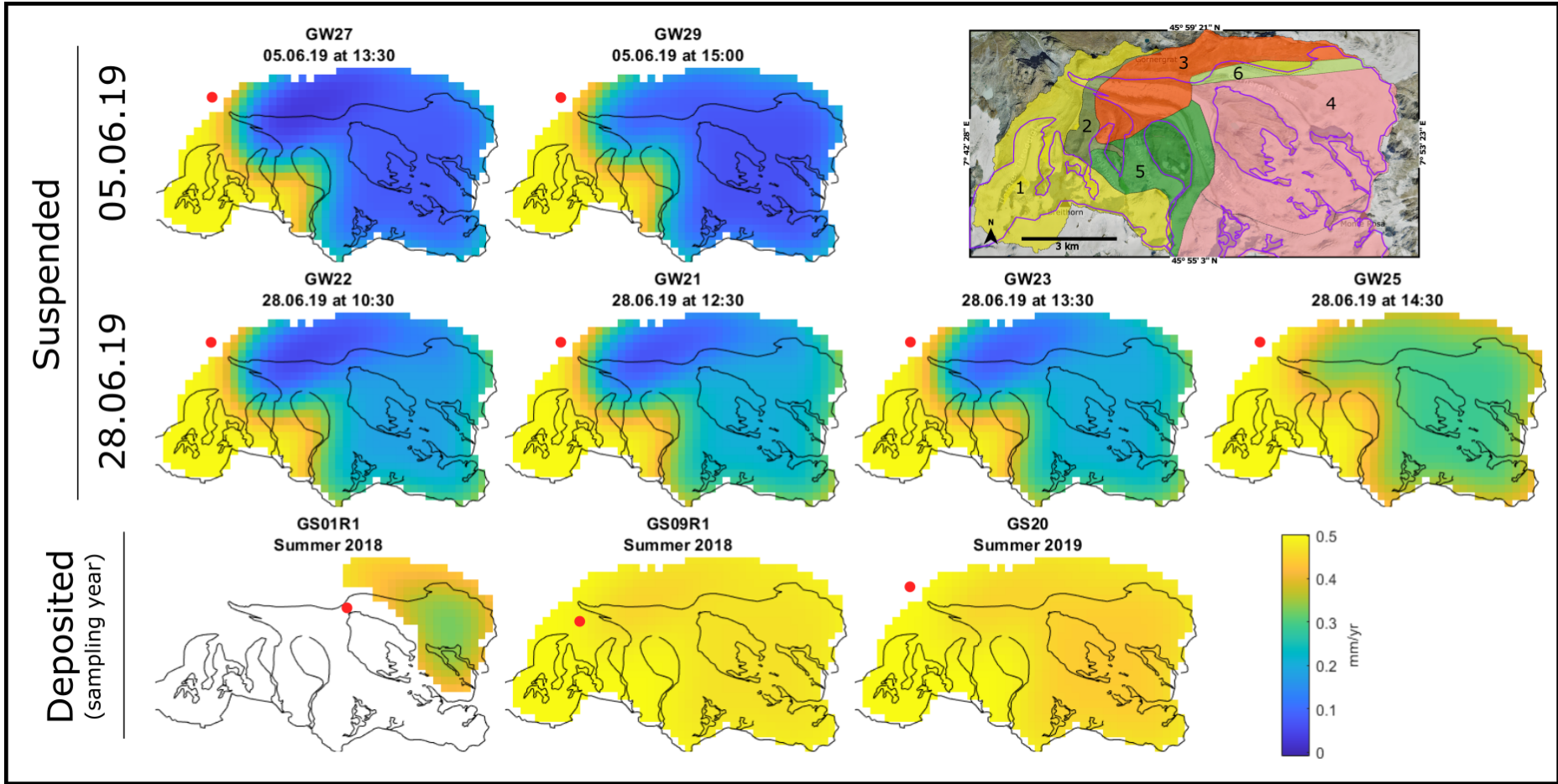


Figure 6: Resulting erosion rates maps for suspended and deposited samples. Red dots correspond to approximate sampling locations.

retreat. In fact, the recently exposed proglacial area is characterized by a large availability of sediments (especially ground moraine) in unstable conditions, which were uncovered by the retreating glacier and are now easily mobilized and transported by hydraulic and gravitational processes. Fig. 7 shows the glacier's retreat from 1982 to 2020 and, as is the case for most Alpine glaciers, the greatest morphological changes do indeed happen at the glacier's snout, where ice is rapidly lost and the newly exposed surfaces are covered in large quantities of sediments (of which an important part was eroded *in situ*). This interpretation is consistent with Tsyplenkov et al. (2021), whose results suggest that riverbank erosion in the proglacial area is the main contributor of suspended sediments in glacierized catchments, as measured beyond a certain distance from the glacier's snout (in their case, approximately 800 m) and in normal weather conditions. This process is also expected to happen in the area between the recently disconnected Gorner and Grenz glaciers, which encloses large quantities of sediments, constituting a possible source of easily mobilized materials.

5.2.1 Deposited detrital samples

While suspended sediments could arguably be interpreted as direct signals of erosion, deposited sediments (samples GS01R1, GS09R1 and GS20, Fig. 1) are a mix of materials whose deposition times could span many months or years. These sediments have most likely been subject to selective entrainment (by size, density or shape, e.g. Malusà et al., 2016; Garzanti et al., 2009) before and upon deposition, and were hence expected to feature variable zircon concentrations according to their deposition environment/process and consequent predominant grain sizes. Deposited samples were collected from riverbanks in sediment-rich areas above the normal stream discharge level. In these samples, zircon grains are less abundant than originally expected and feature average grain sizes that are larger than in bedrock samples. This leads to believe that their deposition can be attributed to specific - or a series of - high-discharge events, during which grains as small as the ones used for this study (30-70 μm) are unlikely to settle (which would explain their under-representation). The resulting deposits are expected to contain large quantities of re-mobilized, glacial sediments that were eroded and deposited over variable time intervals, whose signals would be interpreted by the model as extremely high erosion rates. Similarly to results from suspended load data, high erosion rates are found for sample GS01R1 close to the Gorner-Grenz intersection (Fig. 6, 7) where a large quantity of sediments is available because of the glacier's retreat. When compared to the other deposited samples, GS01R1 shows lower erosion rates for the higher-elevation part of unit 4, which could be attributed to downstream sediment storage effects. The drainage of *Gornersee* (a glacier-dammed lake that

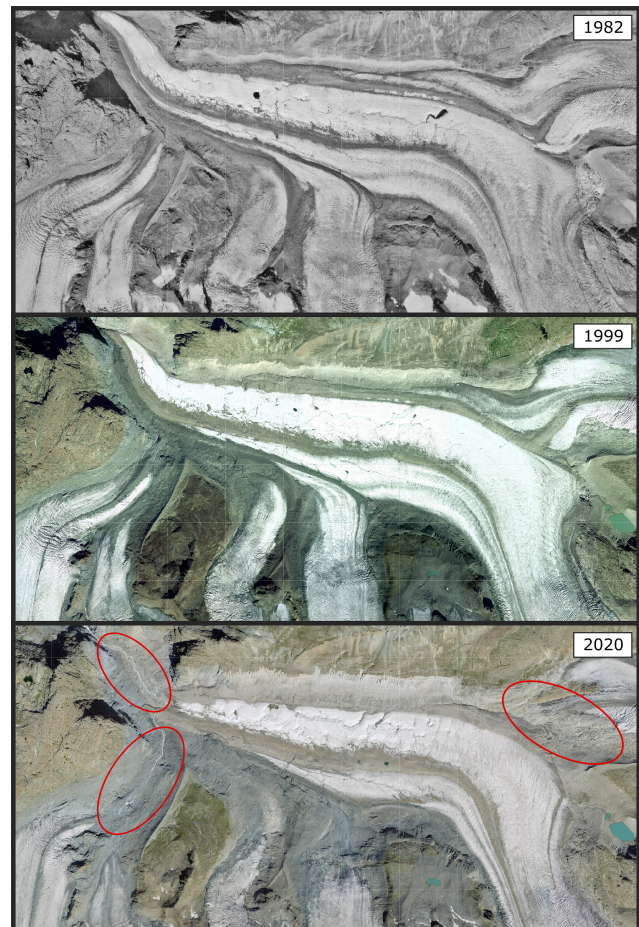


Figure 7: Glacial retreat over the study area since 1982. Red circles highlight newly exposed proglacial areas featuring large quantities of unstable sediments exposed to water- and gravity-driven erosion processes, which are thought to be the main sources of suspended sediments (Swisstopo, 2021).

used to form annually close to the Gorner-Grenz intersection) is thought to be the most likely driver of such high-discharge events. The lake usually appeared in May and drained between June and August, resulting in high discharges and complex dynamic feedbacks (Huss et al., 2007; Sugiyama et al., 2008). Since the outbursts used to happen during the early melting season when the subglacial channel network is relatively under-developed, flushing was effective over the entire bed surface, hence explaining why the erosion rates are higher in deposited samples, while conserving the general patterns specific of each unit. Sediments sampled at the Gorner-Grenz intersection are not influenced by these outbursts (which used to take place downstream) and do hence show lower erosion rates for the eastern part of the catchment, while detecting higher erosion rates on unit 6 where sediments are exposed because of the glacier's retreat.

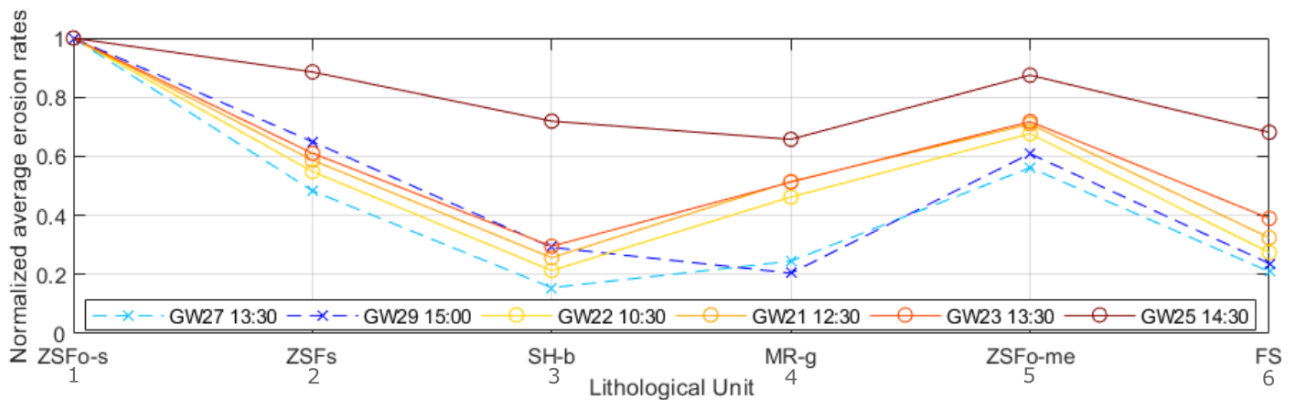


Figure 8: Average contribution of each unit to erosion rates, per sample. Dashed and solid lines are for June 5 and June 28 2019, respectively.

5.2.2 Suspended detrital samples

Differences in erosion rates from suspended samples between the beginning and the end of June represent variations over a period of 23 days during the early melting season. Similarly, since each water sample corresponds to a specific hour of the day, the resulting erosion maps represent short-time variations of erosion rates within that day (2 maps for the afternoon of June 5, and 4 maps spanning late-morning to mid afternoon for June 28). Note that the displayed time is that of the sampling, as no correction for transport time has been done (as mentioned in section 4).

As presented in Table 1, suspended sediments feature much higher zircon concentrations than expected, meaning that zircon grains of the investigated size (30-70 μm) were remarkably abundant in the river's water (most likely because of their specific grain size range). This confirms that, this close to the glacier's terminus, the turbulence of the proglacial stream is sufficient to keep zircon grains in suspension (Bridge & Bennett, 1992). Suspended zircon availability for studies such as this one would hence seem to be assured in high-energy proglacial streams, and can be improved by sampling larger volumes of water (1 to 2 liters per sample, depending on the expected fertility). Regarding the monthly variations (beginning/end of June), Fig. 6 and 8 suggest that either the availability of sediments or the transport capacity in unit 4 (MR-g) and 5 (ZSFo-me) become more efficient throughout the month, which is in line with temperature and discharge data (Fig. 3): the significant raise in average temperatures between the beginning and the end of June is responsible for enhanced ice melt at higher elevations. This increases the supply of meltwater to the ice-bedrock interface, which increases water pressure and therefore increases sliding velocities, erosion rates and the transport capacity of the system (e.g. Hallet, 1979; Hooke, 1991; Riihimaki et al., 2005; Herman et al., 2011; Anderson et al., 2014). Considering that units 4 and 5 lie at generally higher elevations than other units, stored sediments will only be flushed out

later when melting temperatures are reached and meltwater becomes sufficiently available, which seems to be reflected in the erosion rate maps, where the higher parts of the catchment are only activated at the end of June, after an important raise in average temperatures. Fig. 8 offers a more intuitive visualization of this result: the contributions from units 4 (MR-g) and 5 (ZSFo-me) for June 5 are low compared to these on June 28.

5.2.3 Ice velocities and slope contribution

Despite the limited number of analysed grains, hourly evolutions in erosion rates are already detectable for June 5 between 13:30 and 15:00, where a slight increase is visible for unit 3 (SH-b) in the central part of the main Gorner-Grenz tongue. For that day, most units show an increase in relative contributions between the first (13:30) and the second (15:00) sampling times (Fig. 8), which is consistent with increasing discharges (and, consequently, also sediment production and/or transport) throughout the early afternoon. This temporal change in sediment delivery is especially pronounced for units 2 (ZSF-s) and 3 (SH-b), and could be explained by the fact that these units are mainly covered by the lowest part of the Gorner-Grenz tongue (2300 - 2400 m a.s.l.), supposedly the most dynamic part of the glacier this early in the melting season. Unit 4 (MR-g) does not comply with the general trend, as its contribution seems to decrease in time for June 5.

A longer time-series is available for June 28, where the daily evolution is consistent with the less evident results of June 5, included sample GW25 (14:30), even if its erosion rate values look unexpectedly high. While (as discussed earlier) erosion rates stay notoriously high on the western part of the catchment, an increase in the central part of the main Gorner-Grenz tongue is clearly visible from the maps, and Fig. 8 confirms this regular tendency for all units between 10:30 and 13:30. These hourly results match simultaneous discharge measurements, which (for both June 5

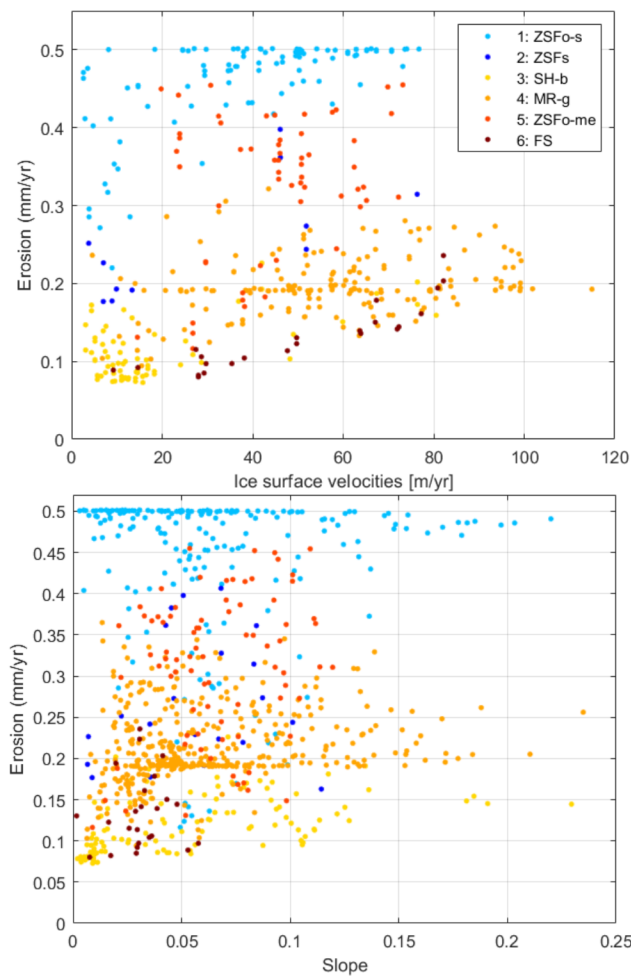


Figure 9: Median resulting erosion rates plotted against a) median slope (for each cell of the model) and b) median ice surface velocities (only for cells where ice is present). While no clear trend is observable between erosion rates and slope in any unit, a slight positive correlation exists between erosion rates and ice surface velocities in units 1, 2, 3 and 6.

and June 28) increase almost linearly throughout the sampling day. However, this means that the abnormally high values in sample GW25 (June 28 at 14:30) could not be explained by discharge variations unless their relation were assumed to be non-linear. Given that different geological units in the system are covered by glaciers which have independent dynamics, it is unlikely that the general increase between 13:30 and 14:30 seen in sample GW25's results be linked to a generalized glacial surge. Such a rapid increase in suspended sediment delivery might in fact be attributable to any threshold-controlled process such as daily melt having finally reached an area higher up in the glacier where sediments are still available, or the evolution of the subglacial draining network. Another reasonable explanation may be a momentary spike in SSCs, po-

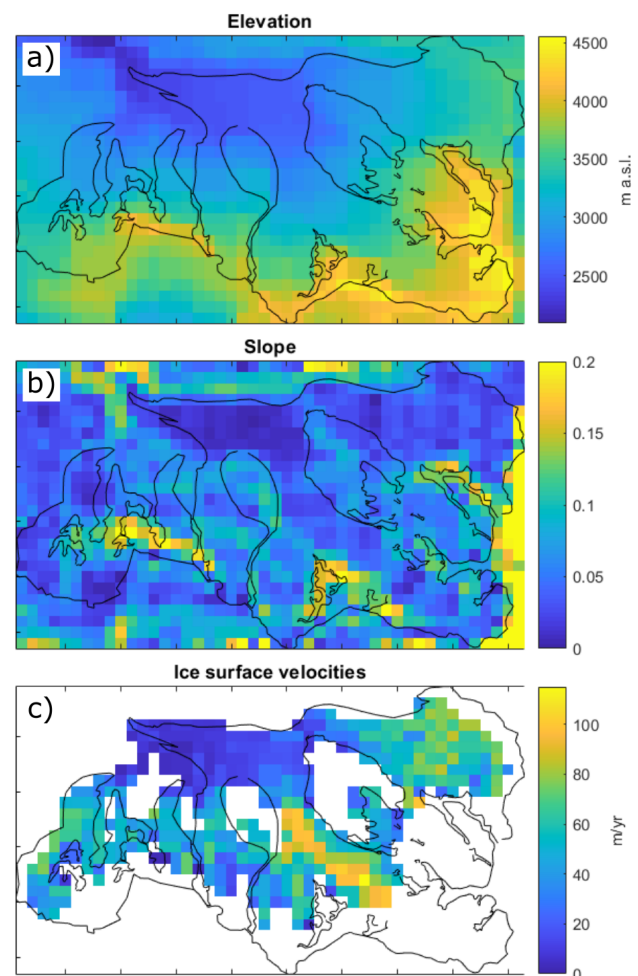


Figure 10: a) Catchment Digital Elevation Model (DEM); b) Catchment slope; c) Ice surface velocities.

tentially missed because of a delay between the sampling of water and the measurement of turbidity. This would imply that the high erosion rates in GW25 might actually be the result of sediment remobilization during a short-lived event linked to subglacial instability, such as a localised collapse of a portion of a channel or riverbank.

Interestingly, as visible in Fig. 8, the increase in contributions from the lower parts of the system (units 2 and 3) is stronger between 13:00 and 15:00 in the beginning of June, than throughout the whole day in the end of June. This is perfectly reasonable if the large discharges linked to the June 9-10 rainfall event are taken into consideration: as opposed to the beginning of June, a significant part of the sediments that were accumulated below the glacier during winter must have been flushed out and are no longer available on June 28. This interpretation also explains why units 2 and 3 show the highest differences, that is because they are located where the overdeepening glacier is thought to store large quantities of sediments as long as water pressure remains low (Swift et al., 2005).

To summarize, both clear temporal and spatial evolutions of erosion rates (over hourly and monthly time intervals) were found, which emphasizes the validity of the model by yielding results that reinforce well-established knowledge on glacial dynamics throughout the early ablation season. As discussed in section 4, higher erosion rates are expected from areas with higher basal sliding velocities [1], but sediment (re)mobilization has most likely an influence on the recorded suspended sediment signal. A third main possible source of sediments is the contribution from surrounding slopes, whose quantification was not attempted here, but whose presence was confirmed by Total Organic Carbon (TOC) analyses: $n = 45$ suspended load samples from the proglacial stream were analysed at UNIL's laboratories by means of a Rock-Eval 6 apparatus, yielding TOC concentrations of up to 2.25%, interpreted as a proxy for slope material contribution. A part of the zircons in the proglacial stream might hence originate from weathering and periglacial erosive processes coupled with general denudation occurring in the surrounding slopes, rather than from below the glacier, and would hence represent signals of slope denudation instead of sole subglacial processes. In order to investigate these links, an existing surface velocity map of the glacier (Fig. 10c) has been used as a proxy for basal sliding velocities, and surface velocities of each glacierized cell in the model have been plotted against erosion rates (Fig. 9). The same has been done for slope and erosion rates for each cell in the model, where (if present) the external contribution was expected to be somehow proportional to the steepness of the surrounding slopes. As displayed in Fig. 9, no identifiable trend was found between slope and erosion rates, which suggests that the sampled material should not be directly linked to slope processes, whereas surface velocities show slightly positive (although not conclusive) correlations for all units except 4 and 5. Such a pattern, however weak, is in contrast with expectations based on [1], as higher erosion rates should have been associated with faster-flowing ice, namely units 5 and 6. It should be considered that the Gorner-Grenz ice flow has been observed to feature complex dynamic behaviour, which might bias the choice of using ice surface velocities as a proxy for sliding velocity patterns. Namely, Ryser et al. (2013) suggest that the presence of cold ice in the ablation area (possibly coupled with the influence of Gornersee, Riesen et al., 2010) might complicate the glacier's dynamics making it difficult to describe its flow via classical ice flow models. Nevertheless, such anomalies could not explain alone the almost absence of correlations between ice velocities and erosion, meaning that (while showing little contribution from general slope processes) the model is most likely biased by the signal of sediment remobilization in deglaciated areas, especially from the proglacial plains of individual glaciers in the system, and other recently deglaciated areas such as the former Gorner-Grenz in-

terception.

6 Conclusions

Spatio-temporal variations of sediment delivery patterns at Gornergletscher (Switzerland) were reconstructed for the early melting season of 2019 by means of an inversion model using zircon ages from suspended load as tracers, with the aim of investigating glacial erosion rates and subglacial sediment dynamics. The solving of the inverse problem was possible because of prior knowledge about the spatial distribution of subglacial source areas (geological units): U-Pb geochronology on bedrock zircons yielded very distinct age distributions, which allowed for a straightforward separation into age bins (the model's fingerprints), and suspended zircons in the proglacial stream were found to be sufficiently large and abundant to be selected and dated via LA-ICPMS, totaling approximately 750 processed grains among bedrock, suspended and deposited samples. The results of the model are one catchment map per detrital sample where colors indicate spatially varying erosion rates. Given that samples were collected at different times, maps can be read as spatial evolutions of erosion rates in time. This work presents and discusses results over monthly and hourly timescales during the early melting season (several maps per day are generated for June 5 and June 28, 2019). Results suggest that the major contributor to suspended load is the proglacial area where the glacier's retreat has made available large quantities of sediments for transport, and meltwater as well as other denudation processes can easily mobilize them. This seems to be the case, in different proportions, for the proglacial areas of all glaciers in the system (which are nowadays disconnected). Suspended sediment signals in the proglacial stream could not be attributed to one main erosive process, but suggest that products of direct glacial erosion and those of sediment remobilization are simultaneously present in variable proportions. No clear link between erosion rates and ice flow velocities was identified, and the contribution from surrounding hillslope was confirmed but appears to remain negligible in normal weather conditions. According to results, the major driving mechanisms of suspended sediment delivery are thought to be transport capacity and the characteristics and evolution of the subglacial draining network, as well as the location of sediment stocks: different areas are activated at different times during the early melting season, most likely as a result of flushing events associated with strong rainfalls. Moreover, hourly evolutions of erosion rates within the same day were observed to adopt non-linear behaviors during the afternoon, which might be attributable to threshold-controlled processes such as daily melt having finally reached specific locations higher up in the glacier where sediments are still available, or the evolution of the subglacial draining network. Erosion maps

were also generated for zircons from deposited sediments collected in 2018 and 2019 in the proglacial areas of Gorner and Grenz glaciers from locations that are not in direct contact with river dynamics under normal discharge conditions. These appear to have been deposited by major high-discharge events, which for Gornergletscher are probably associated with the seasonal drainage of a glacier-dammed lake (Gornersee). Further research is necessary to assess the contribution of direct bedrock glacial erosion to total suspended sediment delivery, possibly coupled with simultaneous estimates of sliding velocities at the glacier scale. Although zircon ages proved to be valid tracers, it is recommended to sample larger volumes of water in order to ensure grain availability and statistical representativeness for all source areas. Moreover, water samples should be collected as close to the glacier as possible, in order to minimize the influence of proglacial sediment dynamics. Sampling water from several locations in the catchment (e.g. from the Gorner-Grenz intersection) would hopefully allow to pinpoint sediment storage areas within the glacier and assist in the interpretation of erosion and mobilization processes through time.

7 Data availability

The MATLAB inversion code (De Doncker et al., 2020) and all other data used for obtaining this thesis' results are available at https://github.com/bbelotti/erosion_zircon_inversion.

8 Acknowledgements

I wish to thank Prof. Frédéric Herman¹ for giving me the opportunity to join his research and for supervising my work. I am grateful to Fien De Doncker¹ and Dr. Günther Prasicek¹ for their valuable contributions and help, and to Prof. Sébastien Castelltort² for joining the evaluation committee as an external expert. Also, I thank Michelle Foley³, Alexey Ulyanov³, Caroline De Meyer³, Othmar Müntener³ and Benita Putlitz³ for their precious technical support.

¹ UNIL, Institute of Earth Surface Dynamics;

² UNIGE, Department of Earth Sciences;

³ UNIL, Institute of Earth Sciences.

References

- Andersen, T. (2005). Detrital zircons as tracers of sedimentary provenance: limiting conditions from statistics and numerical simulation. *Chemical Geology*, 216(3-4), 249–270.
- Anderson, B., Willis, I., Goodsell, B., Banwell, A., Owens, I., Mackintosh, A., & Lawson, W. (2014). Annual to daily ice velocity and water pressure variations on ka roimata o hine hukatere (franz josef glacier), new zealand. *Arctic, Antarctic, and Alpine Research*, 46(4), 919–932.
- Aoki, S., Aoki, K., Tsuchiya, Y., & Kato, D. (2019). Constraint on the eclogite age of the sanbagawa metamorphic rocks in central shikoku, japan. *International Geology Review*, 61(18), 2211–2226.
- Bridge, J. S., & Bennett, S. J. (1992). A model for the entrainment and transport of sediment grains of mixed sizes, shapes, and densities. *Water Resources Research*, 28(2), 337–363.
- Collins, D. N. (1990). Seasonal and annual variations of suspended sediment transport in meltwaters draining from an alpine glacier. *IAHS Publ*, 193, 439–446.
- De Doncker, F. (2019). *Short term glacial erosion of the gorner glacier: constraining the relation between basal sliding velocity and glacial erosion*. Leuven: KU Leuven. Faculteit Wetenschappen.
- De Doncker, F., Herman, F., & Fox, M. (2020). Inversion of provenance data and sediment load into spatially varying erosion rates. *Earth Surface Processes and Landforms*, 45(15), 3879–3901.
- Delaney, I., Bauder, A., Werder, M. A., & Farinotti, D. (2018). Regional and annual variability in subglacial sediment transport by water for two glaciers in the swiss alps. *Frontiers in Earth Science*, 6, 175.
- Eisen, O., Bauder, A., Lüthi, M., Riesen, P., & Funk, M. (2009). Deducing the thermal structure in the tongue of gornergletscher, switzerland, from radar surveys and borehole measurements. *Annals of Glaciology*, 50(51), 63–70.
- FOEN. (n.d.). *Meteoswiss GIN database*. Retrieved 2021, from <https://www.gin5.admin.ch/gin>
- Garzanti, E., Andò, S., & Vezzoli, G. (2009). Grain-size dependence of sediment composition and environmental bias in provenance studies. *Earth and Planetary Science Letters*, 277(3-4), 422–432.
- Gehrels, G. (2011). Detrital zircon u-pb geochronology: Current methods and new opportunities. *Tectonics of sedimentary basins: Recent advances*, 45–62.
- Guillon, H., Mugnier, J.-L., Buoncristiani, J.-F., Carcaillet, J., Godon, C., Prud'Homme, C., ... Vassallo, R. (2015). Improved discrimination of subglacial and periglacial erosion using 10be concentration measurements in subglacial and supraglacial sediment load of the bossons glacier (mont blanc massif, france). *Earth Surface Processes and Landforms*, 40(9), 1202–1215.
- Gurnell, A., Hannah, D., & Lawler, D. (1996). Suspended sediment yield from glacier basins. *IAHS Publications-Series of Proceedings and Reports-Intern Assoc Hydrological Sciences*, 236, 97–104.
- Hallet, B. (1979). A theoretical model of glacial abrasion. *Journal of Glaciology*, 23(89), 39–50.
- Hallet, B. (1996). Glacial quarrying: A simple theoretical model. *Annals of Glaciology*, 22, 1–8.
- Hallet, B., Hunter, L., & Bogen, J. (2013). Rates of erosion and sediment evacuation by glaciers. *Fluv Geom: Geom Crit Conc Vol*, 12, 213–35.
- Haritashya, U. K., Kumar, A., & Singh, P. (2010). Particle size characteristics of suspended sediment transported in meltwater from the gangotri glacier, central himalaya—an indicator of subglacial sediment evacuation. *Geomorphology*, 122(1-2), 140–152.
- Herman, F., Beaud, F., Champagnac, J.-D., Lemieux, J.-M., & Sternai, P. (2011). Glacial hydrology and erosion patterns: a mechanism for carving glacial val-

- leys. *Earth and Planetary Science Letters*, 310(3-4), 498–508.
- Herman, F., Beyssac, O., Brughelli, M., Lane, S. N., Leprieux, S., Adatte, T., ... Cox, S. C. (2015). Erosion by an alpine glacier. *Science*, 350(6257), 193–195.
- Herman, F., Braun, J., Deal, E., & Prasicek, G. (2018). The response time of glacial erosion. *Journal of Geophysical Research: Earth Surface*, 123(4), 801–817.
- Hooke, R. L. (1991). Positive feedbacks associated with erosion of glacial cirques and overdeepenings. *Geological Society of America Bulletin*, 103(8), 1104–1108.
- Horstwood, M. S., Košler, J., Gehrels, G., Jackson, S. E., McLean, N. M., Paton, C., ... others (2016). Community-derived standards for la-icp-ms u-(th)-pb geochronology—uncertainty propagation, age interpretation and data reporting. *Geostandards and Geoanalytical Research*, 40(3), 311–332.
- Huss, M., Bauder, A., Werder, M., Funk, M., & Hock, R. (2007). Glacier-dammed lake outburst events of gornersee, switzerland. *Journal of Glaciology*, 53(181), 189–200.
- Jackson, S. (2008, 01). Lamtrace data reduction software for la-icp-ms. *Laser Ablation ICP-MS in the Earth Sciences: Current Practices and Outstanding Issues*, 40.
- Koiter, A., Owens, P., Petticrew, E., & Lobb, D. (2013). The behavioural characteristics of sediment properties and their implications for sediment fingerprinting as an approach for identifying sediment sources in river basins. *Earth-Science Reviews*, 125, 24–42.
- Koppes, M., Hallet, B., Rignot, E., Mouginot, J., Wellner, J. S., & Boldt, K. (2015). Observed latitudinal variations in erosion as a function of glacier dynamics. *Nature*, 526(7571), 100–103.
- MacGregor, K. R., Anderson, R. S., & Waddington, E. D. (2009). Numerical modeling of glacial erosion and headwall processes in alpine valleys. *Geomorphology*, 103(2), 189–204.
- Malusà, M. G., Resentini, A., & Garzanti, E. (2016). Hydraulic sorting and mineral fertility bias in detrital geochronology. *Gondwana Research*, 31, 1–19.
- Matlab [Computer software manual]. (2018). Natick, Massachusetts.
- Prasicek, G., Mettra, F., Lane, S., & Herman, F. (2020). Recent patterns of discharge and sediment output of the gorner glacier, switzerland. In *Egu general assembly conference abstracts* (p. 9242).
- Riesen, P., Sugiyama, S., & Funk, M. (2010). The influence of the presence and drainage of an ice-marginal lake on the flow of gornergletscher, switzerland. *Journal of Glaciology*, 56(196), 278–286.
- Riihimäki, C. A., MacGregor, K. R., Anderson, R. S., Anderson, S. P., & Loso, M. G. (2005). Sediment evacuation and glacial erosion rates at a small alpine glacier. *Journal of Geophysical Research: Earth Surface*, 110(F3).
- Ryser, C., Lüthi, M., Blindow, N., Suckro, S., Funk, M., & Bauder, A. (2013). Cold ice in the ablation zone: Its relation to glacier hydrology and ice water content. *Journal of Geophysical Research: Earth Surface*, 118(2), 693–705.
- Schaeffli, B., Hingray, B., & Musy, A. (2007). Climate change and hydropower production in the swiss alps: quantification of potential impacts and related modelling uncertainties. *Hydrology and Earth System Sciences*, 11(3), 1191–1205.
- Schoene, B. (2014). 4.10-u-th-pb geochronology. *Treatise on geochemistry*, 4, 341–378.
- Steck, A., Masson, H., & Robyr, M. (2015). Tectonics of the monte rosa and surrounding nappes (switzerland and italy): Tertiary phases of subduction, thrusting and folding in the pennine alps. *Swiss Journal of Geosciences*, 108(1), 3–34.
- Sugiyama, S., Bauder, A., Huss, M., Riesen, P., & Funk, M. (2008). Triggering and drainage mechanisms of the 2004 glacier-dammed lake outburst in gornergletscher, switzerland. *Journal of Geophysical Research: Earth Surface*, 113(F4).
- Swift, D. A., Nienow, P. W., & Hoey, T. B. (2005). Basal sediment evacuation by subglacial meltwater: suspended sediment transport from haut glacier d'arolla, switzerland. *Earth Surface Processes and Landforms*, 30(7), 867–883.
- Swisstopo. (2021). *Maps of switzerland*. Retrieved 2021-02-05, from <https://map.geo.admin.ch/>
- Tarantola, A. (2005). *Inverse problem theory and methods for model parameter estimation*. SIAM.
- Tarantola, A., & Valette, B. (1982). Generalized nonlinear inverse problems solved using the least squares criterion. *Reviews of Geophysics*, 20(2), 219–232.
- Tsyplenkov, A., Vanmaercke, M., Collins, A. L., Kharchenko, S., & Golosov, V. (2021). Elucidating suspended sediment dynamics in a glacierized catchment after an exceptional erosion event: The djankuat catchment, caucasus mountains, russia. *CATENA*, 203, 105285.
- Ugelvig, S. V., Egholm, D. L., & Iverson, N. R. (2016). Glacial landscape evolution by subglacial quarrying: A multiscale computational approach. *Journal of Geophysical Research: Earth Surface*, 121(11), 2042–2068.
- Werder, M., Schuler, T. V., & Funk, M. (2010). Short term variations of tracer transit speed on alpine glaciers. *The Cryosphere*, 4(3), 381–396.
- Widmann, P., Davies, J., & Schaltegger, U. (2019). Calibrating chemical abrasion: Its effects on zircon crystal structure, chemical composition and upb age. *Chemical Geology*, 511, 1–10.